

Competing fracture modes in brittle materials subject to concentrated cyclic loading in liquid environments: Trilayer structures

Ilja Hermann and Sanjit Bhowmick

Materials Science and Engineering Laboratory, National Institute of Standards and Technology, Gaithersburg, Maryland 20899-8500

Yu Zhang

Department of Biomaterials and Biomimetics, New York University College of Dentistry, New York, New York 10010

Brian R. Lawn^{a)}

Materials Science and Engineering Laboratory, National Institute of Standards and Technology, Gaithersburg, Maryland 20899-8500

(Received 19 August 2005; accepted 11 November 2005)

A study is made of top-surface cracks induced in brittle trilayers by cyclic indentation with a hard sphere in water. The trilayers consist of an external brittle layer (veneer) fused to an inner stiff and hard ceramic support layer (core), in turn adhesively bonded to a thick compliant base (substrate). These structures are meant to simulate essential aspects of dental crowns, but their applicability extends to a range of engineering coating systems. The study follows on from like studies of brittle monoliths and brittle-plate/soft-substrate bilayers. Competing fracture modes in the outer brittle layer remain the same as before: outer and inner cone cracks and radial cracks, all of which form in the near-contact zone and propagate downward toward the veneer/core interface. Inner cone cracks and radial cracks are especially dangerous because of their relatively steep descent through the outer layer as well as enhanced susceptibility to mechanical fatigue. Experiments are conducted on model glass/alumina/polycarbonate systems, using video cameras to record the fracture evolution in the transparent glass layer in situ during testing. Each fracture mode can lead to failure, depending on the maximum contact load and other variables (plate thickness, sphere radius). The potentially beneficial role of a stiff intervening core is discussed, along with potentially deleterious side effects of residual thermal-expansion-mismatch stresses.

I. INTRODUCTION

Two preceding papers have described the competition between top-surface fracture modes in monolith brittle materials¹ and bilayers consisting of a brittle coating on a compliant substrate (bilayer)² subjected to cyclic contact loading in liquids. The study is now extended to trilayers with a stiff, hard ceramic layer between the external brittle coating and the compliant substrate. Such trilayers are highly relevant to the performance of veneer/core dental crowns on dentin,^{3,4} as well as to a variety of other engineering multilayer coating structures, where the intermediate “core” layer is meant to provide support for an otherwise weaker (but functional) outer “veneer”

layer.⁵ In those two preceding papers, three crack modes shown schematically in Fig. 1 were identified: outer cone cracks (O), inner cone cracks (I), and medial–radial cracks (R). Cyclic loading in water enhances these modes, especially the I cracks—by a hydraulic pumping mechanism—and the R cracks—by accumulated quasi-plasticity.^{6,7} As in bilayers, these top-surface fracture modes may be expected to result in through-thickness failures. Additional fracture modes depicted in Fig. 1 may also operate^{8–10}: delamination at weak interlayer interfaces (D), or radial cracking at the ceramic bottom surface (R_{*}). However, although such modes can be significant in dental layer structures under certain conditions, we will defer detailed consideration of these alternative modes to a later study.

The current paper describes cyclic experiments on model trilayers aimed at investigating the effect of an intermediate support layer on top-surface crack modes.¹¹

^{a)}Address all correspondence to this author.

e-mail: brian.lawn@nist.gov
DOI: 10.1557/JMR.2006.0056

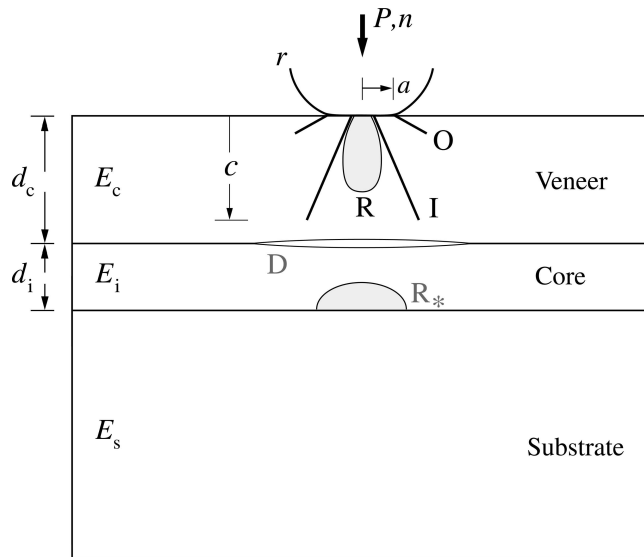


FIG. 1. Schematic illustration of crack geometry for cyclic contact on brittle double layer bonded to compliant support base with sphere of radius r at load P , contact radius a , and number of cycles n . Showing top-surface crack modes in veneer, through-thickness depth c : outer cone cracks (O), inner cone cracks (I), and radial cracks (R). Additional radial cracks (R_*) can occur at core bottom surface, and delamination (D) at the interface, but these are secondary in this study.

The trilayers are fabricated by first fusing 1 mm soda-lime glass outer layers (representative of dental porcelain) onto 0.5 mm alumina support layers (representative of dental cores). The glass/alumina combination represents a large modulus difference, and is therefore ideally suited to highlight elastic mismatch effects. Residual stresses from thermal expansion mismatch are sufficiently small as to permit interlayer bonding with minimal spontaneous delamination (as is generally the case in dental crowns) but are not entirely negligible in the fracture mechanics, as we shall see. Then the fused glass/alumina double layers are adhesively bonded onto a polycarbonate base with a thin epoxy resin interlayer to simulate dentin support for cemented crowns in real tooth structures. The glass top surfaces are subsequently subjected to cyclic contact loading with tungsten carbide spheres in water, in simulation of occlusal function. The ensuing crack evolution is observed in situ, from initiation to penetration through to the glass/alumina interface (failure). As with the monoliths and bilayers, it will be shown that each of the O, I and R cracks can dominate under certain conditions. Of these, I and R cracks are particularly dangerous, especially after prolonged cycling at lower contact loads.

II. EXPERIMENTAL

The layer specimen configuration used was a slightly modified version of that described in earlier studies.^{2,8,11,12} Soda-lime glass plates $25 \times 25 \times 1$ mm of

Young's modulus 70 GPa were retained for the upper (veneer) layer. The plates were pre-abraded at their top surfaces with grade 600 SiC grit to provide a uniform density of flaw sites for crack initiation. (This is not inconsistent with clinical practice in the finishing of dental crowns, where the dentist uses a diamond burr to grind the occlusal surfaces to provide a perfect bite.¹³) Side faces were polished to enable side viewing during subsequent testing. Alumina plates $12 \times 12 \times 0.5$ mm of modulus 370 GPa (AD995, CoorsTek, Golden, CO) were used for the bottom (core) support layer. These were polished to avoid bottom-surface R_* cracks (Fig. 1).¹⁴

The outer coating (c) soda-lime glass and inner support (i) alumina plates were then fused together to form a double layer of thickness $d_c + d_i = 1.5$ mm (typical of crown layer dimensions^{11,15}). The fusion was effected using an adhesive glass tape (G-1001 transfer tape, Vitta Corp, Bethel, CT) heated to 600 °C, producing an interfacial glass layer of thickness ≈ 50 μm . The tape material was chosen to closely match the modulus and coefficient of thermal expansion (CTE) of the soda-lime glass to minimize residual stresses (see Appendix). The glass-tape fusion process was intended to produce a chemical bond of sufficiently high strength to avoid interfacial D cracks (Fig. 1). Nevertheless, the fused bilayers showed some detectable bending, with glass surface concave, indicating significant residual stresses. In less than 5% of the specimens the glass layer actually fractured during the processing, suggesting that the intensity of any such residual stresses can reach an appreciable fraction of the glass strength.

The glass/alumina ceramic bilayers were then bonded to a compliant polycarbonate slab 12.5 mm thick (Hyzod, AIN Plastics, Norfolk, VA) with a thin (<20 μm) layer of epoxy resin adhesive (Harcos Chemicals, Bellesville, NJ), whose properties closely match those of the polycarbonate.⁸ With respect to the glass coating, insertion of an intermediate alumina layer may be conveniently regarded as increasing the effective modulus of the supporting substrate,¹⁶ a notion to which we shall return in Sec. IV.

Contact testing and in situ side viewing of the crack evolution were carried out as previously described.^{1,2} A small WC indenter of radius $r = 1.58$ mm was used to ensure dominant top-surface damage. (In an earlier study, larger indenters of radius $r \approx 4$ mm were used to suppress top-surface damage so as to enable preferential R_* cracking at the alumina bottom surface.¹¹) Cyclic loading was carried out in half-sine mode at frequency 1 Hz in a fatigue testing machine (Model 5500R, Instron Corp., Canton, MA), with maximum loads ranging from $P_m = 75$ N up to 500 N. A minimum load slightly higher than zero was used in all cases to prevent the indenter losing contact with the specimen surface and “wandering” during cycling. All such tests were conducted in a

perpetual water surface film, replenished drop by drop at the contact site throughout the duration of the experiment. Using a video camera set up for side viewing, crack depths c were recorded at the deepest points of penetration for each crack type as a function of number of cycles n . Failure was deemed to occur when the first of these cracks intersected the glass/alumina interface, at which point the experiment was stopped. The O cracks appeared first, usually in the first contact cycle. Again, as previously, some difficulty was experienced in observing the initial stages of the I and R cracks, but the ensuing propagation stages were clearer once these cracks penetrated below the base rim of the preceding outer cones. A second video camera placed below the specimen was used to confirm the absence of any bottom-surface R* cracks in these experiments.

Some auxiliary Vickers indentation tests were conducted on the glass plates both before and after fusion with the alumina core layers, to assess the existence of any residual CTE stresses from corner crack length measurements (Appendix).

III. RESULTS

A. Crack morphology

The observed crack morphologies for the three cracking modes were similar to those for bilayers,² except that the failure condition in the trilayers was markedly more disruptive. Side-view video frames for each mode are given in Fig. 2: (a) O crack, load $P_m = 500$ N, number of cycles to failure $n_F = 58$ cycles; (b) I crack, $P_m = 200$ N, $n_F = 13625$ cycles; (c) R crack, $P_m = 120$ N, $n_F = 3790$ cycles. Only the top glass layer is shown. The frames in Fig. 2 are those immediately prior to through-thickness penetration. A systematic change in dominant crack mode with diminishing load is apparent. Characteristic features are shallow O cone cracks [Fig. 2(a)], steeper I cones with water-filled segments [Fig. 2(b)], and kidney-shaped R radial cracks again with ingressing water [Fig. 2(c)]. Because of the water intrusion, the latter two crack types were sometimes difficult to distinguish, requiring rotation of the camera axis to determine a 3D picture of the geometry. At higher loads ($P_m = 500$ N) O cracks were the only ones to form, and propagated unstably to failure after penetrating only $\approx 25\%$ of the glass thickness. At lower loads, O cracks formed first but were overtaken by their I and R competitors after prolonged cycling. These latter cracks, although accelerating through the lower half of the glass layer, approached the glass bottom surface more stably than in the bilayers—note the I and R cracks have achieved $\approx 90\%$ penetration without failure in Figs. 2(a) and 2(b). However, once the cracks reached the glass/alumina interface, failure was marked by sudden expansion into a multiple

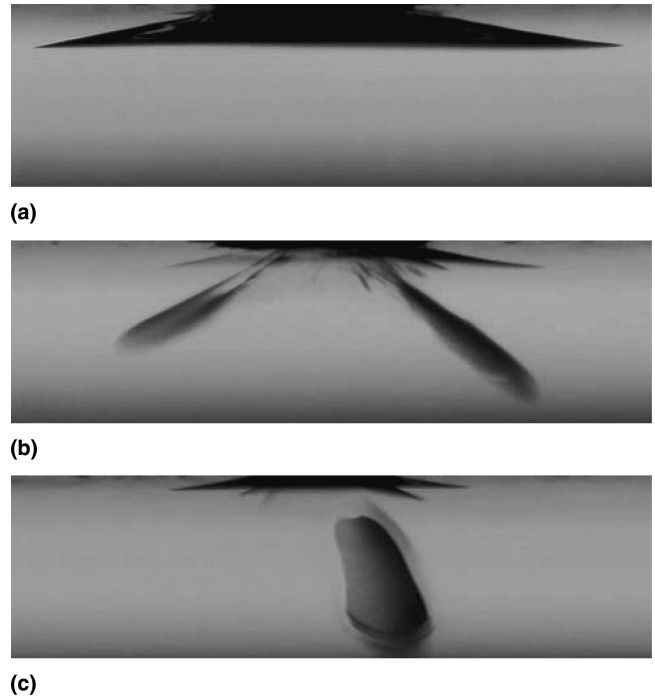


FIG. 2. Side views of near-failures from Hertzian indentation sites in soda-lime glass plate of thickness $d_c = 1$ mm bonded to alumina plate thickness $d_i = 0.5$ mm on polycarbonate base during cycling at 1 Hz in water with WC spheres of radius $r = 1.58$ mm. Only the glass plate is shown. In all three cases, the images are video frames immediately prior to crack penetration through the glass layer: (a) outer O cone crack at $P_m = 500$ N after $n_F = 58$ cycles, (b) inner I cone crack at $P_m = 200$ N after $n_F = 13625$ cycles, and (c) median-radial crack at $P_m = 120$ N after $n_F = 3790$ cycles.

fracture mode, including delamination. At this point the cracks proliferated and spread rapidly to the edges of the specimen, making any post-mortem analysis difficult.

In our experiments, there was no indication that any of the cracks initiated in the glass ever penetrated into the adjoining alumina. In selected specimens, removal of the fractured glass top layer, either spontaneously by delamination at failure or by subsequent prying of fractured glass fragments from the alumina layer followed by HF etch, confirmed this. Thus the alumina layer remained intact and crack free under the test conditions here.

B. Crack evolution

The crack evolution $c(n)$ for different crack modes in glass/alumina/polycarbonate trilayers is compared in Fig. 3 for (a) O, (b) I and (c) R cracks at specified loads P_m . In all cases the cycling was stopped when any one crack penetrated fully through the glass thickness, indicated by the horizontal dashed line. Each symbol represents a different specimen. Note that in some cases it is not always the same fracture mode that leads to failure, e.g., I and R data at $P_m = 120$ N in Figs. 3(b) and 3(c).

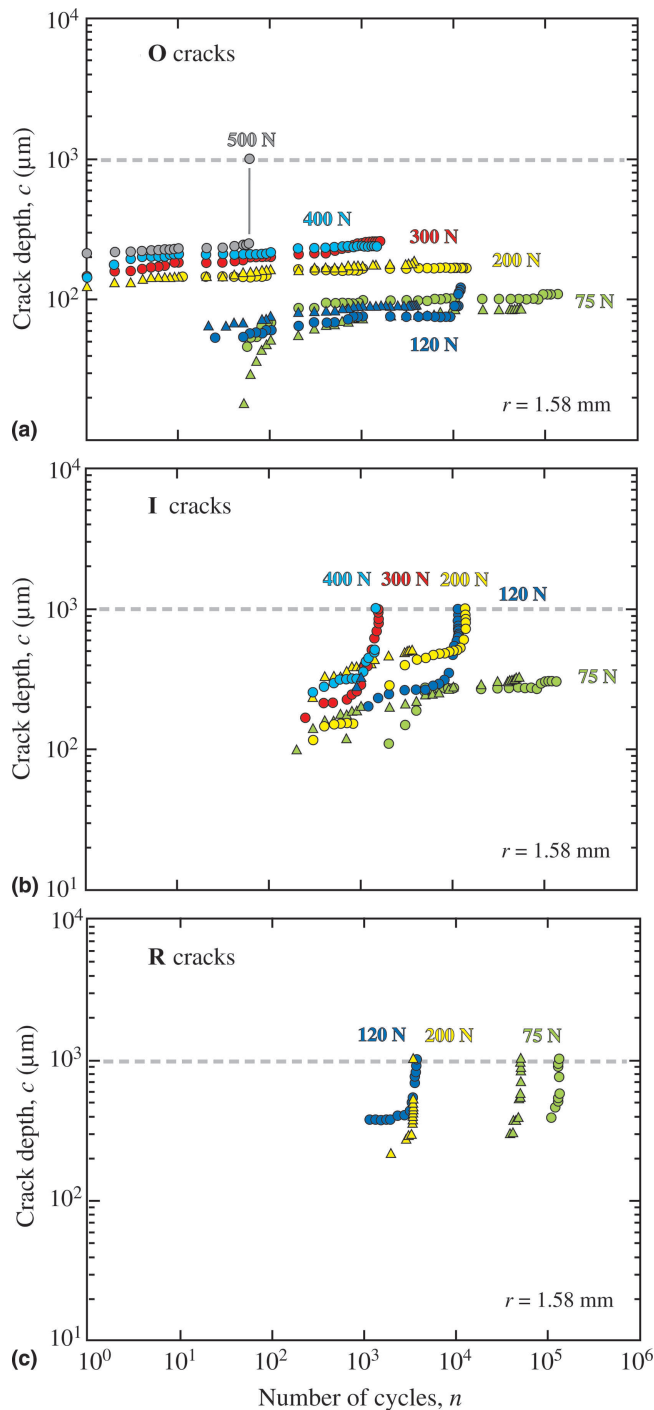


FIG. 3. Crack depth c for soda-lime-glass/alumina/polycarbonate trilayers, $d_c = 1$ mm and $d_i = 0.5$ mm, as function of number of cycles n for indentation with WC sphere of radius $r = 1.58$ mm, frequency 1 Hz, in water. Data for (a) outer cone cracks O, (b) inner cone cracks I, and (c) radial cracks R. Each color represents a different load P , each symbol a different indentation. Note how O cracks form first but are ultimately overtaken by I and R cracks.

Over the load range covered here, O cracks always initiate first, at $n = 1$ for $P_m > 120$ N and between $n = 1$ and 100 for $P_m < 120$ N. At $P_m = 500$ N, O cracks [Fig. 3(a)] are the only ones to form, and grow steadily to

a depth $c \approx 250 \mu\text{m}$ before abrupt failure (vertical line). At $P_m < 500$ N, the O cracks remain stable and approach a steady state $c \sim n^{2/3N}$ (with crack velocity exponent $N = 17.9$ for soda-lime glass) at large n without ever achieving failure, much as in glass monoliths.¹ In this latter load region, I cracks [Fig. 3(b)] then R cracks [Fig. 3(c)] become visible after $n \approx 10^2$ to 10^4 cycles, depending on the value of P_m , and constitute the dominant sources of failure. The I and R cracks approach the failure condition less abruptly than their O crack counterparts, in most cases remaining stable up to the point of full penetration of the glass layer but with little indication of attaining a steady state in $c(n)$. At $P_m < 120$ N, the R cracks tend to become the dominant mode for this particular combination of glass and alumina thicknesses.

It is instructive to compare $c(n)$ responses for trilayers with those from the earlier monolith and bilayer studies. Such comparisons are made in Figs. 4, 5, and 6 at $P_m = 200$, 120, and 75 N, respectively, for (a) glass monolith ($d_c = \infty$),¹ (b) glass/polycarbonate bilayer ($d_c = 1$ mm, $d_i = 0$),² and (c) glass/alumina/polycarbonate trilayer ($d_c = 1$ mm, $d_i = 0.5$ mm). Again, dashed lines indicate glass layer thicknesses. The acceleration of each crack type through the lower half of the glass plates in the layer structures, especially in the case of the I and R cracks, is once more apparent. At $P_m = 200$ N (Fig. 4) failure occurs at larger numbers of cycles in the trilayer than the bilayer. Note also that the approach of the cracks to the interface is less abrupt in the trilayer. These trends are as may be anticipated for a system with a more rigid support base, attributable to reduced flexure in the glass layer. At $P_m = 120$ N (Fig. 5) the trends are similar, with a relative shift in all $c(n)$ data sets toward larger n . However, in this case the critical number of cycles to failure for the trilayer is about the same as for the bilayer. At $P_m = 75$ N (Fig. 6), the data shift to even higher n continues, but now with failure occurring at smaller number of cycles in the trilayer than in the bilayer. These latter trends would appear to contradict the notion of enhanced support from the alumina layer. We will argue later that such a reverse shift may be explained by the presence of modest residual CTE mismatch stresses.

C. Critical conditions for failure

Consider now the conditions for failure of the trilayers ($d_c = 1$ mm, $d_i = 0.5$ mm), corresponding to number of cycles $n = n_F$ at which cracks intersect the glass/alumina interface as a function of cyclic load P_m , plotted in Fig. 7 as the filled symbols. For comparison, previous data for bilayers ($d_c = 1$ mm, $d_i = 0$) are included as the unfilled symbols.² At $P_m \geq 500$ N, O cracks initiate and lead to failure within the first cycle (not indicated in the figure), and therefore dominate in this region. O cracks continue to dominate at P_m just below 500 N, with strong

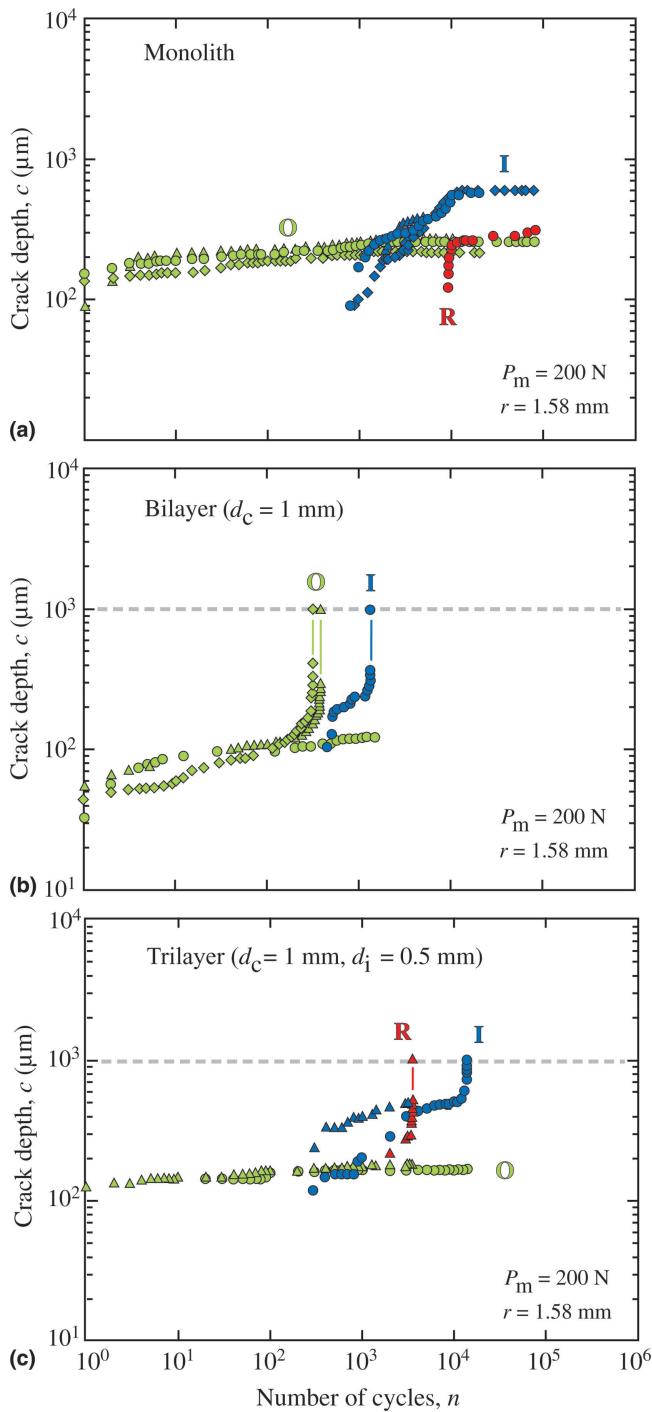


FIG. 4. Crack depth c for soda-lime-glass/alumina/polycarbonate trilayers as function of number of cycles n for indentation with WC sphere of radius $r = 1.58$ mm, frequency 1 Hz, in water. Data for (a) monolith glass, (b) bilayer glass/polycarbonate, and (c) trilayer glass/alumina/polycarbonate. Tests at maximum load $P_m = 200$ N. Each color represents a different crack mode, each symbol a different indentation. Data in (a) from Zhang et al.¹ and in (b) from Bhowmick et al.²

dependence of n_F on P_m . At lower loads, I and R cracks begin to dominate, with strongly diminishing slope in the $n_F(P_m)$ dependence. Note a significant shift to higher n_F in the trilayer data relative to the bilayer data at high and

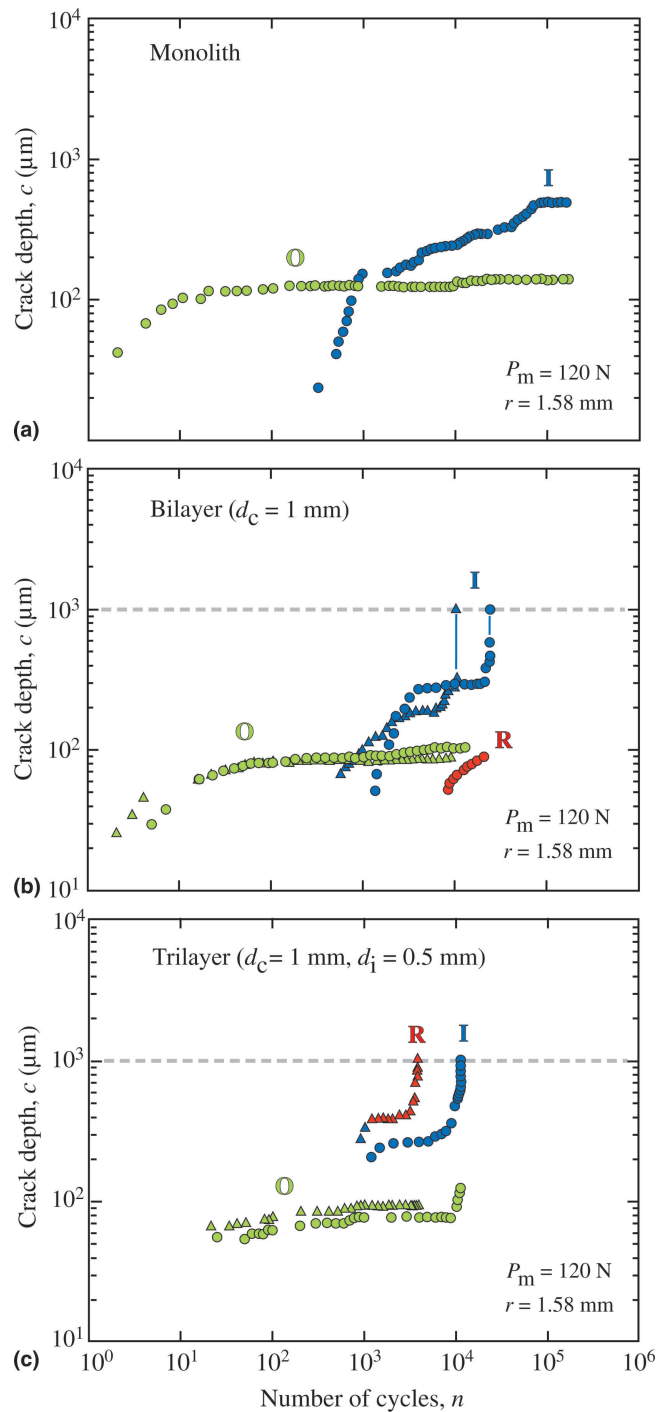


FIG. 5. Crack depth c for soda-lime-glass/alumina/polycarbonate trilayers as function of number of cycles n for indentation with WC sphere of radius $r = 1.58$ mm, frequency 1 Hz, in water. Data for (a) monolith glass, (b) bilayer glass/polycarbonate, and (c) trilayer glass/alumina/polycarbonate. Tests at maximum load $P_m = 120$ N. Each color represents a different crack mode, each symbol a different indentation. Data in (a) from Zhang et al.¹ and in (b) from Bhowmick et al.²

intermediate values of P_m . Again, this is consistent with the notion of additional support from the alumina core layer, suppressing the flexure that enhances crack instability. However, at low P_m , the data for trilayers and

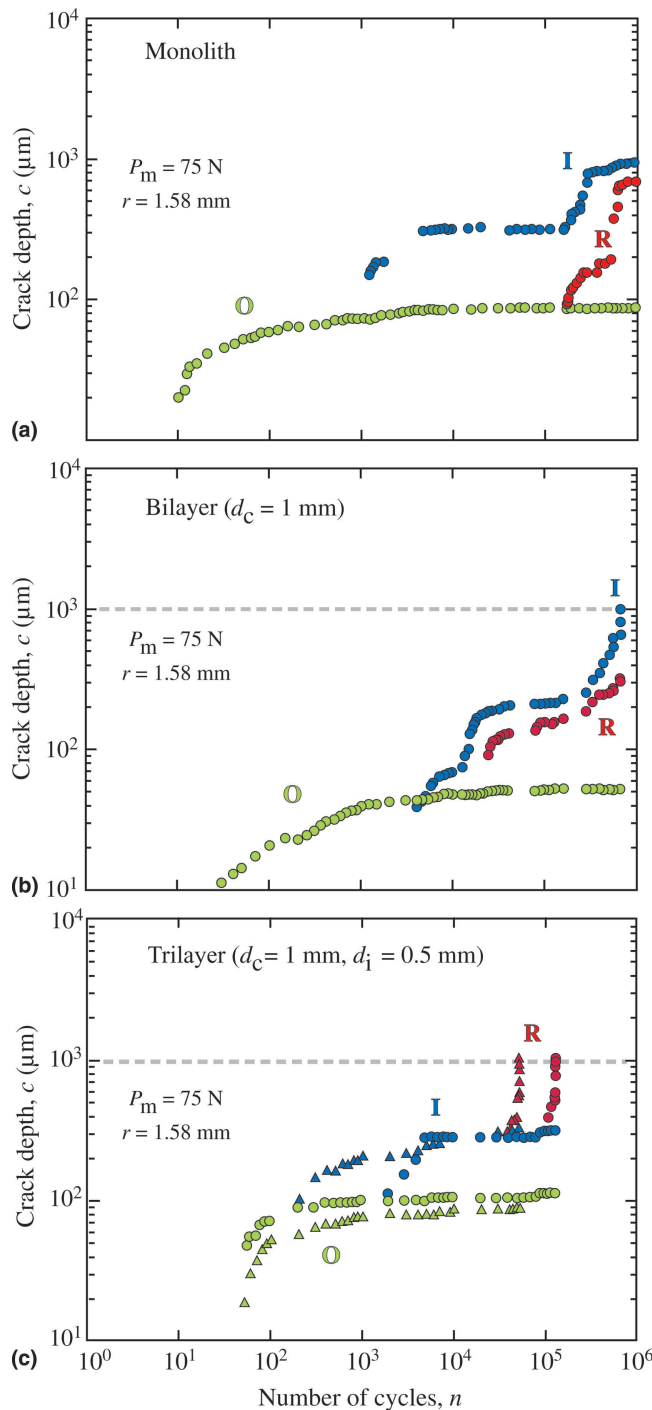


FIG. 6. Crack depth c for soda-lime-glass/alumina/polycarbonate trilayers as function of number of cycles n for indentation with WC sphere of radius $r = 1.58$ mm, frequency 1 Hz, in water. Data for (a) monolith glass, (b) bilayer glass/polycarbonate, and (c) trilayer glass/alumina/polycarbonate. Tests at maximum load $P_m = 75$ N. Each color represents a different crack mode, each symbol a different indentation. Data in (a) from Zhang et al.,¹ and in (b) from Bhowmick et al.²

bilayers appear to merge and even cross; i.e., failure is easier in the trilayer than it is in the bilayer, attributed in the consideration of Fig. 6 to side effects from thermal mismatch stresses.

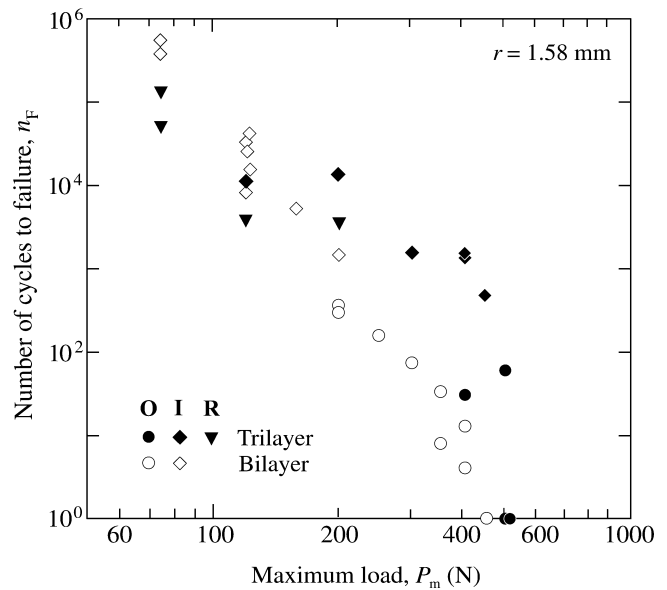


FIG. 7. Number of cycles to failure n_F as function of maximum contact load P_m , for glass/alumina/polycarbonate trilayers ($d_c = 1$ mm, $d_i = 0.5$ mm). Data for glass/polycarbonate bilayers ($d_c = 1$ mm) included for comparison.² Note failure from different crack modes at different P_m .

IV. DISCUSSION

In this study we have examined the competition between cracks driven by blunt contact in glass “veneer” layers fused onto alumina “core” layers, in turn bonded to compliant polycarbonate support layers, in a water environment. Such layer structures are pertinent to practical engineering laminates, especially all-ceramic dental crowns. The fracture modes are the same as those observed in monoliths and bilayers. Inclusion of the stiff alumina core layer shifts the $c(n)$ data for trilayers relative to bilayers toward longer lifetimes in Figs. 4 and 5 (but not Fig. 6; see below), consistent with reduced flexure in the glass veneer layer. Generally in our material system O cracks initiate first but are responsible for failure only at the highest loads. At intermediate and lower loads, I and R cracks initiate after prolonged cycling and overtake their predecessors, becoming the dominant sources of failure. Use of glass as a model layer material for in situ observation enables us to follow the progress of these new cracks directly. Even then, observation of the I and R cracks is not easy, especially in the initial stages, partly because of shielding by the preceding O cracks and partly because of the intrusion of water; on occasion, it is even difficult to distinguish between the I and R cracks. In opaque materials, labor-intensive specimen sectioning may be the only practical way of confirming the existence of any such subsurface cracks prior to failure.¹⁷ These difficulties in monitoring the subsurface crack evolution, coupled with the relatively swift progression to failure (recall again the absence of

pronounced steady-state $c(n)$ plateaus in Figs. 3–6, render the I and R modes extremely dangerous in cyclic loading.

Further consideration may be given to the role of the alumina as a support core layer for the overlying glass (or, in dental crowns, for porcelain). We may quantify this role by considering the system as a “reduced bilayer,” with a top glass plate of modulus E_c supported by a single-material substrate of effective modulus E_s^* , as depicted in Fig. 8. The quantity E_s^* for our material systems may be evaluated using individual modulus values. For the monolith, the “substrate” has the same modulus as the overlayer, $E_s^* = E_c = 70$ GPa (all-glass continuum). For the bilayer, $E_s^* = E_s = 2.3$ GPa (glass plate on polycarbonate support). For the trilayer, the effective modulus of the composite alumina/polycarbonate substrate may be evaluated using an empirical rule of mixtures, $E_s^* = E_i(E_c/E_i)^L$, where $L = \exp\{-[1.18 + 0.33\log(d_i/d_c)]^{3.13}\}$.¹⁶ Inserting $E_i = 370$ GPa and $E_s = 2.3$ GPa, $d_c = 1$ mm and $d_i = 0.5$ mm, yields $E_s^* = 90$ GPa. Hence the support for the glass plate in the trilayer is determined to be considerably higher than in the bilayer and a little higher than in the monolith. This would account for the longer lifetimes of trilayers across the upper and intermediate load range in Fig. 7. However, it does not account for the merging of trilayer and bilayer data at the lower end of the load range in Fig. 7, nor for the enhanced instabilities in trilayers relative to monoliths at all loads in Figs. 4–6. This suggests some additional factor operating in the trilayers.

As foreshadowed, one such factor is residual stress from thermal expansion mismatch between the glass and alumina. Although we have attempted to minimize this mismatch in our specimens, even small differentials can give rise to significant stresses during cooling.¹⁸ An evaluation for our glass/alumina laminates is given in the Appendix, using finite element analysis in conjunction with Vickers indentation measurements. We find that the stress in the glass switches from -33 MPa (compression) at the top surface to $+66$ MPa (tension) at the interface. This level of tensile stress is about half the strength of our glass⁸ but nonetheless sufficient to exert a pronounced destabilizing influence on the growth of the downward

extending cracks in the lower half of the glass plate in the trilayers relative to bilayers; i.e., as the stress-intensity factor $K_R \sim \sigma_R c^{1/2} F(c/d)$ associated with residual stress σ_R across the glass section (F a rising function of c/d) begins to dominate the term $K_H \sim P/c^{3/2}$ associated with Hertzian contact. Such superposed residual stresses will be expected to become more dominant at lower indentation loads (e.g., Figs. 6 and 7), due to diminution of the Hertzian field (lower P), thus accounting for shortened lifetimes in trilayers relative to bilayers. A detailed quantitative evaluation of the residual stress influence would require a more complete analysis of the fracture mechanics of the I and R modes, including incorporation of hydraulic pumping and quasiplasticity driving forces (over and above the pervasive effects of slow crack growth) than is currently available.² Suffice it to say that residual tensile stresses in the lower half of the veneer pose a threat to the survival of any trilayer system, if not from the veneer itself then from the core, a fact appreciated by dental technicians for whom interlayer CTE matching remains a prime requisite in crown fabrication.

Some material and environmental aspects of the trilayer system are worth reinforcing here. In our experiments glass is used as the model brittle top layer. As discussed previously in our preceding paper on glass monoliths¹ the I fracture mode operates only in the presence of liquid water in the vicinity of the contact, and is more likely to occur in harder ceramics, favoring more brittle behavior. The R mode is favored in softer, coarser ceramics, where enhanced quasiplasticity can occur, but does not necessarily require a liquid environment (although water certainly does enhance quasiplastic damage accumulation). We have seen that in glass (and, by association, porcelain) veneers, conditions are such that both I and R modes can be mutually competitive. Changes in the core and substrate materials can also significantly influence the crack evolution by virtue of their effect on the support modulus E_s^* , although not always beneficially.

Our attention in this study has focused on cracks initiating from the near-contact region at the top surface. As alluded to in Sec. I, additional fracture modes may dominate under certain conditions (Fig. 1). Delamination D

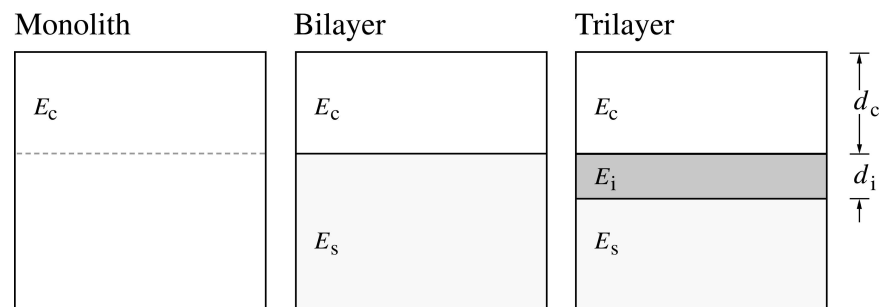


FIG. 8. Schematic illustration showing ceramic monolith, ceramic/substrate bilayer, and ceramic/intermediate-layer/substrate.

cracks may occur if the toughness of the veneer/core interface is sufficiently lower than that of the bulk core material.¹⁹ In our case, the tough alumina core precludes penetration of the cracks across the interface, so that delamination is the only course. However, in our experiments delamination only occurs after the transverse cone or radial cracks have penetrated the glass layer, and in that sense plays a secondary role in the failure process. Potentially more devastating are radial cracks R_* that initiate at the bottom surface of the core ceramic. These are most likely to occur in trilayers with smaller veneer-core net thickness, i.e., $d = d_c + d_i < 1$ mm, or with heavily abraded core undersurfaces (e.g., from severe sandblasting/abrasion), or in systems with cores of relatively low strength.¹¹ There is a need to consider such additional modes in designing structures for maximum failure resistance. While acknowledging their importance, we will defer detailed consideration to a later study.

Other variables may play important roles in the failure conditions. Some of these have already been examined in the preceding papers on monoliths and bilayers.^{1,2} One such variable is the nature of the contact. In the present experiments we have exclusively used a WC sphere of radius $r = 1.58$ mm. Using an indenter of higher radius or lower modulus will diminish the Hertzian stress intensity at any given load, effectively shifting the $c(n)$ data in Figs. 3–6 to the right, i.e., toward longer lifetimes.^{1,2} This is of special interest in the context of dental crowns, where contacts typically occur over larger cuspal radii and with like tooth/crown (enamel/porcelain) opposing moduli. Another important variable is the relative veneer/core layer thickness d_c/d_i for a fixed net thickness $d = d_c + d_i$. Will a lower value of veneer thickness d_c promote premature failure, primarily because the crack has less distance to travel to the interface but also because of redistribution of tensile residual stresses? Conversely, will a larger value of d_i provide greater support for the veneer layer? Likewise, what will be the effect of modulus difference E_c/E_i ? These are issues for future study.

We may conclude that addition of a stiff, tough intermediate layer, by providing enhanced elastic support for the outer layer and an arrest barrier for penetrating cracks, can moderately (but not universally) increase the resistance to failure from top-surface damage.

ACKNOWLEDGMENTS

This work was supported by a grant from the National Institute of Dental and Craniofacial Research (PO1 DE10976). Discussions with Herzl Chai (University of Tel Aviv) and assistance with Oriented Finite Element Analysis (OOF) calculations (Appendix) by Stephen Langer (National Institute of Standards and Technology) are gratefully acknowledged.

REFERENCES

1. Y. Zhang, S. Bhowmick, and B.R. Lawn: Competing fracture modes in brittle materials subject to concentrated cyclic loading in liquid environments: monoliths. *J. Mater. Res.* **20**, 2021 (2005).
2. S. Bhowmick, Y. Zhang, and B.R. Lawn: Competing fracture modes in brittle materials subject to concentrated cyclic loading in liquid environments: Bilayer structures. *J. Mater. Res.* **20**, 2792 (2005).
3. J.R. Kelly, R. Giordano, R. Pober, and M.J. Cima: Fracture surface analysis of dental ceramics: Clinically failed restorations. *Int. J. Prosthodont.* **3**, 430 (1990).
4. J.R. Kelly: Ceramics in restorative and prosthetic dentistry. *Ann. Rev. Mater. Sci.* **27**, 443 (1997).
5. B.R. Lawn, Y. Deng, P. Miranda, A. Pajares, H. Chai, and D.K. Kim: Overview: damage in brittle layer structures from concentrated loads. *J. Mater. Res.* **17**, 3019 (2002).
6. Y. Zhang, J.-K. Kwang, and B.R. Lawn: Deep penetrating conical cracks in brittle layers from hydraulic cyclic contact. *J. Biomed. Mater. Res.* **73B**, 186 (2005).
7. H. Chai and B.R. Lawn: Hydraulically pumped cone fractures in brittle solids. *Acta Mater.* **53**, 4237 (2005).
8. H. Chai, B.R. Lawn, and S. Wuttiphon: Fracture modes in brittle coatings with large interlayer modulus mismatch. *J. Mater. Res.* **14**, 3805 (1999).
9. Y.-W. Rhee, H.-W. Kim, Y. Deng, and B.R. Lawn: Contact-induced damage in ceramic coatings on compliant substrates: Fracture mechanics and design. *J. Am. Ceram. Soc.* **84**, 1066 (2001).
10. Y. Deng, B.R. Lawn, and I.K. Lloyd: Characterization of damage modes in dental ceramic bilayer structures. *J. Biomed. Mater. Res.* **63B**, 137 (2002).
11. Y. Deng, P. Miranda, A. Pajares, F. Guiberteau, and B.R. Lawn: Fracture of ceramic/ceramic/polymer trilayers for biomechanical applications. *J. Biomed. Mater. Res.* **67A**, 828 (2003).
12. B.R. Lawn, Y. Deng, and V.P. Thompson: Use of contact testing in the characterization and design of all-ceramic crown-like layer structures: A review. *J. Prosthet. Dent.* **86**, 495 (2001).
13. Y. Zhang, B.R. Lawn, K.A. Malament, V.P. Thompson, and E.D. Rekow: Damage accumulation and fatigue life of sandblasted dental ceramics. (unpublished).
14. Y. Zhang, B.R. Lawn, E.D. Rekow, and V.P. Thompson: Effect of sandblasting on the long-term strength of dental ceramics. *J. Biomed. Mater. Res.* **71B**, 381 (2004).
15. J.R. Kelly: Clinically relevant approach to failure testing of all-ceramic restorations. *J. Prosthet. Dent.* **81**, 652 (1999).
16. J.H. Kim, P. Miranda, D.K. Kim, and B.R. Lawn: Effect of an adhesive interlayer on the fracture of a brittle coating on a supporting substrate. *J. Mater. Res.* **18**, 222 (2003).
17. D.K. Kim, Y.-G. Jung, I.M. Peterson, and B.R. Lawn: Cyclic fatigue of intrinsically brittle ceramics in contact with spheres. *Acta Mater.* **47**, 4711 (1999).
18. M.G. Abrams and D.J. Green: Prediction of crack propagation and fracture in residually stressed glass as a function of the stress profile and flaw size distribution. *J. Europ. Ceram. Soc.* (in press).
19. M.-W. He and J.W. Hutchinson: Crack deflection at an interface between dissimilar elastic materials. *Int. J. Solids Struct.* **25**, 1053 (1989).
20. T.W. Clyne: Residual stresses in thick and thin surface coatings, in *Encyclopedia of Materials Science and Technology* (Elsevier, Oxford, U.K., 2001).
21. L.B. Freund and S. Suresh: *Thin Film Materials: Stress, Defect Formation and Surface Evolution* (Cambridge University Press, Cambridge, UK, 2004), Chap. 2.
22. D.B. Marshall and B.R. Lawn: An indentation technique for meas-

uring stresses in tempered glass surfaces. *J. Am. Ceram. Soc.* **60**, 86 (1977).

23. S. Wuttiphon, B.R. Lawn, and N.P. Padture: Crack suppression in strongly bonded homogeneous/heterogeneous laminates: A study on glass/glass-ceramic bilayers. *J. Am. Ceram. Soc.* **79**, 634 (1996).
24. L.M. Braun, S.J. Bennison, and B.R. Lawn: Objective evaluation of short-crack toughness-curves using indentation flaws: Case study on alumina-based ceramics. *J. Am. Ceram. Soc.* **75**, 3049 (1992).

APPENDIX: EVALUATION OF RESIDUAL THERMAL EXPANSION MISMATCH STRESSES

Layer structures are subject to residual stresses from thermal expansion mismatch. The stresses are of order $\Delta\alpha\Delta T$, where $\Delta\alpha = \alpha_c - \alpha_i$ is the differential expansion coefficient between coating (c) and inner support (i) layers and ΔT is the cooling temperature interval.^{18,20,21} These stresses may not distribute uniformly across the layer sections, owing to relaxation of the structure during cooling. Most of the stress redistribution in our trilayer system will come from the relatively stiff glass and alumina, with relatively small contributions from the intervening glass tape and even less from shrinkage of the epoxy used to bond to the compliant polycarbonate base. Accordingly, we focus attention on a simple glass/alumina bilayer here.

An immediate indication that such residual stresses exist can be obtained using Vickers indentations, from the relative sizes of corner cracks on glass top surfaces in trilayer and monolith specimens. Such a comparison is shown in Fig. A1. (The monolithic glass was subjected to the same heat treatment as that used in fusing to the alumina, to ensure similar thermal histories.) The crack lengths are clearly shorter in the trilayer than in the monolith, indicating a compressive stress in the former. An estimate of these stresses can be made from the fracture mechanics relation for Vickers cracks of radial dimension c formed at load P in a uniform field σ_R ²²:

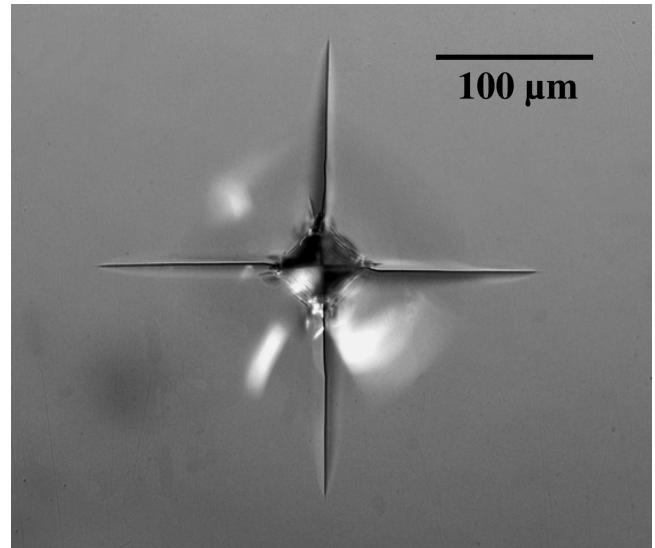
$$K = \psi\sigma_R c^{1/2} + \chi P/c^{3/2} = K_c, \quad (\text{A1})$$

where ψ and χ are crack-geometry and elastic-plastic coefficients, respectively, and K_c is toughness. Equation (A1) can be rearranged to give

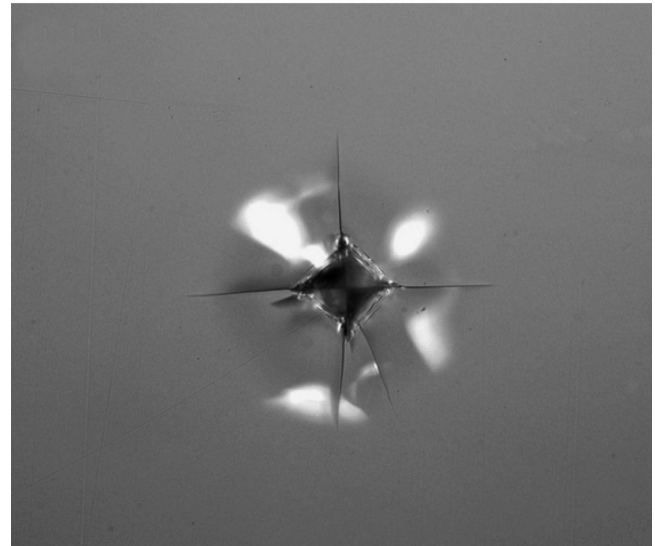
$$\sigma_R = (K_c/\psi c^{1/2})[1 - (c_0/c)^{3/2}] \quad (\text{A2})$$

where c_0 is the corresponding crack length in the control monolith specimen ($\sigma_R = 0$). This relation remains a reasonable approximation as long as the crack lengths c remain small compared to the glass thickness d_c . Inserting $c_0 = 133 \mu\text{m}$ and $c = 93 \mu\text{m}$ from Fig. A1 (mean distances from indentation center to crack tip), $K_c = 0.5 \text{ MPa m}^{1/2}$ (effective toughness of glass in laboratory atmosphere),²³ $\psi = 1$ (average of several evaluations),²⁴ Eq. (A2) yields $\sigma_R(\text{surface}) = -33 \text{ MPa}$.

In this work, we are more concerned with the residual stresses within the glass at the internal interface, i.e.,



(a)



(b)

FIG. A1. Vickers indentations in glass surface, in (a) monolith and (b) trilayer specimen, indentation load 10 N.

$\sigma_R(\text{interface})$. These stresses can be obtained for simple bilayers using analytical formalisms,²¹ but here we use a simple finite element code [Object Oriented Finite Element Analysis (OOF), available for download at <http://www.ctcms.nist.gov/oof/>.] Although the OOF analysis is strictly two-dimensional, the calculations are expected to reflect the stress distributions in axisymmetrically loaded plates. Input parameters are: for glass, $d_c = 1 \text{ mm}$, $E_c = 70 \text{ GPa}$, and $\nu = 0.22$ for glass; for alumina, $d_c = 0.5 \text{ mm}$, $E_i = 370 \text{ GPa}$, and $\nu = 0.22$; cooling temperature range $\Delta T = 600 \text{ }^\circ\text{C}$. Values of $\sigma_R(\text{surface})$ thus computed as a function of $\Delta\alpha$ are plotted in Fig. A2. The data point represents $\sigma_R(\text{surface}) = -33 \text{ MPa}$ measured from the indentation experiments, corresponding to

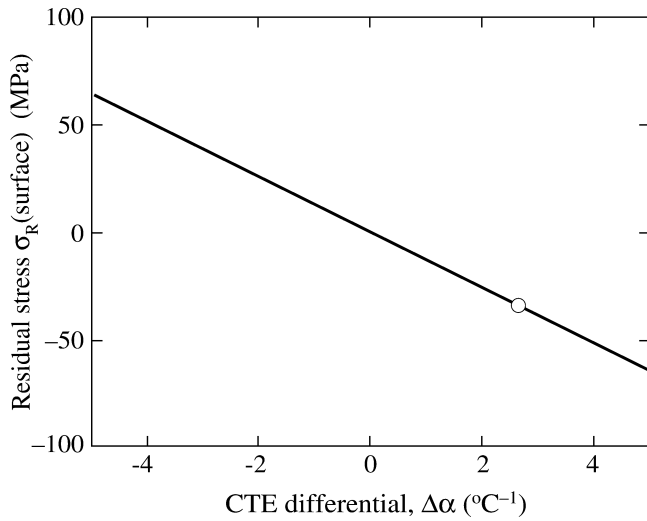


FIG. A2. Plot of residual stress σ_R in trilayer glass surface, as a function of differential expansion coefficient $\Delta\alpha$. The data point indicates surface compressive stress for the trilayer system.

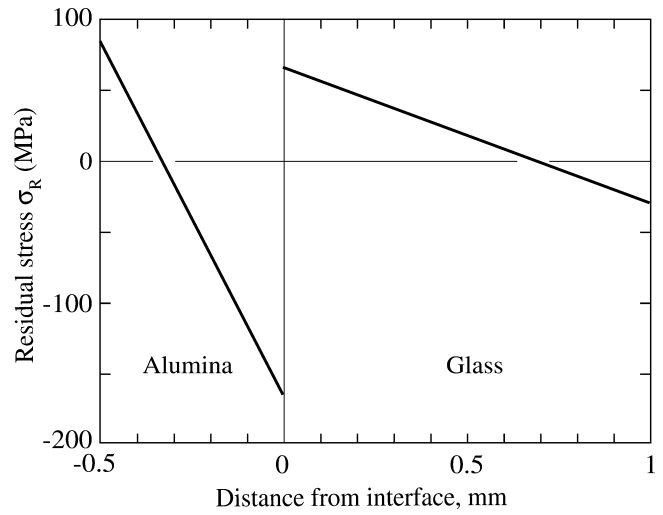


FIG. A3. Distribution of residual stress σ_R across glass/alumina section, for $\Delta\alpha = -2.3 \times 10^{-6} \text{ }^\circ\text{C}^{-1}$, cooling temperature interval $\Delta T = 600 \text{ }^\circ\text{C}$. Note how stress changes sign between outer surface and interior interface.

$\Delta\alpha = -2.3 \times 10^{-6} \text{ }^\circ\text{C}^{-1}$. Figure A3 plots values of σ_R across the bilayer section for this value of $\Delta\alpha$. From this plot, we see that $\sigma_R(\text{interface}) = -2\sigma_R(\text{surface}) = +66 \text{ MPa}$, i.e., a substantial tensile stress. The calculations indicate a resultant small bending of the bilayer, with the glass surface on the concave side, in line with experimental observation in Sec. II.

The value of $\Delta\alpha = \alpha_c - \alpha_i = -2.3 \times 10^{-6} \text{ }^\circ\text{C}^{-1}$ is not inconsistent with literature values for expansion coefficients. For alumina, $\alpha_i \approx 8 \times 10^{-6} \text{ }^\circ\text{C}^{-1}$ (manufacturer's specification). For soda-lime glass the value is dependent

on composition, and typically ranges within $\alpha_c \approx 7$ to $10 \times 10^{-6} \text{ }^\circ\text{C}^{-1}$. Our results would suggest a value of α_c toward the upper limit of this range.

An advantage of the OOF calculations is that they are readily extended to more complex geometries, e.g., incorporating an intervening glass tape interlayer between glass and alumina. Such calculations including an interlayer of thickness $50 \text{ }\mu\text{m}$ with the same modulus as soda-lime glass but expansion coefficient $8.4 \times 10^{-6} \text{ }^\circ\text{C}^{-1}$ (manufacturer specification) changes the stress values in this case by less than 10%.